HHS Public Access

Author manuscript

Eur Urol. Author manuscript; available in PMC 2025 May 20.

Published in final edited form as:

Eur Urol. 2025 March ; 87(3): 342–354. doi:10.1016/j.eururo.2024.10.024.

Molecular Heterogeneity and Immune Infiltration Drive Clinical Outcomes in Upper Tract Urothelial Carcinoma

Kwanghee Kim[a,†,*], **Syed M. Alam**[b,†], **Fengshen Kuo**[a,c], **Ziyu Chen**[c], **Wesley Yip**[b], **Andrew B. Katims**[b], **Carissa Chu**[b], **Andrew T. Lenis**[b], **Wenhuo Hu**[c], **Gamze Gokturk Ozcan**[d], **Jie-Fu Chen**[d], **Sanaz Firouzi**[a], **Yuval Elhanati**[e], **Timothy N. Clinton**[b], **Andreas Aulitzky**[a], **Nima Almassi**[b], **Yoich Fujii**[f], **Andrew T. Tracey**[b], **Peter A. Reisz**[b], **Sadna Budhu**[g], **Lynda Vuong**[a,c], **Jordan Eichholz**[e], **Hyung Jun Woo**[h], **Lucas Nogueira**[a], **Sizhi P. Gao**[c], **Avigdor Scherz**[i], **David H. Aggen**[j], **Jonathan E. Rosenberg**[j], **Eugene J. Pietzak**[b], **Venkatraman Seshan**[e], **Benjamin Greenbaum**[e], **Anton Becker**[k], **Oguz Akin**[k], **Gopa Iyer**[j], **Hikmat Al-Ahmadie**[d], **A. Ari Hakimi**[b,c], **Taha Merghoub**[g], **David B. Solit**[c,h,j,‡,*], **Jonathan A. Coleman**[b,‡,*]

[a]Department of Surgery, Memorial Sloan Kettering Cancer Center, New York, NY, USA;

[b]Urology Service, Department of Surgery, Memorial Sloan Kettering Cancer Center, New York, NY, USA;

[c]Human Oncology and Pathogenesis Program, Memorial Sloan Kettering Cancer Center, New York, NY, USA;

[d]Department of Pathology and Laboratory Medicine, Memorial Sloan Kettering Cancer Center, New York, NY, USA;

[e]Department of Epidemiology-Biostatistics, Memorial Sloan Kettering Cancer Center, New York, NY, USA;

[f]Department of Pathology and Tumor Biology, Kyoto University, Kyoto, Japan;

[*]Corresponding authors. Department of Surgery, Memorial Sloan Kettering Cancer Center, 417 East 68th Street, New York, NY 10065, USA. Fax: +1 646 888 3266 (K. Kim); Urology Service, Department of Surgery, Memorial Sloan Kettering Cancer Center, 353 E. 68th Street, New York, NY 10065, USA. Fax: +1 212 452 3323 (J.A. Coleman); Human Oncology and Pathogenesis Program and Department of Medicine, Memorial Sloan Kettering Cancer Center, 417 East 68th Street, New York, NY 10065, USA. Fax: +1 646 888 3266 (D.B. Solit). kimk1@mskcc.org (K. Kim) solitd@mskcc.org (D.B. Solit) colemanj@mskcc.org (J.A. Coleman).

[†]These authors contributed equally to this article.

[‡]These authors contributed equally to this article.

***Author contributions*:** David B. Solit had full access to all the data in the study and takes responsibility for the integrity of the data and the accuracy of the data analysis.

Study concept and design: Kim, Almassi, Solit, Coleman.

Acquisition of data: Kim, Yip, Katims, Chu, Lenis, Hu, Gokturk Ozcan, J-F Chen, Clinton, Aulitzky, Fujii, Tracey, Reisz, Nogueira, Gao.

Analysis and interpretation of data: Kuo, Z. Chen, Firouzi, Elhanati, Eichholz, Woo, Greenbaum, Becker, Akin, Merghoub, Solit, Coleman.

Drafting of the manuscript: Kim, Alam, Kuo, Yip, Katims, Budhu, Vuong.

Critical revision of the manuscript for important intellectual content: Scherz, Aggen, Rosenberg, Pietzak, Seshan, Iyer, Al-Ahmadie, Hakimi, Merghoub, Solit, Coleman.

Statistical analysis: Kuo, Z. Chen, Eichholz, Seshan.

Obtaining funding: Scherz, Merghoub, Solit, Coleman.

Administrative, technical, or material support: None.

Supervision: Merghoub, Solit, Coleman.

Other: None.

Supplementary material

Supplementary data to this article can be found online at https://doi.org/10.1016/j.eururo.2024.10.024.

[g]Ludwig Collaborative and Swim Across America Laboratory, Department of Pharmacology and Mayer Cancer Center, Weill Cornell Medicine, New York, NY, USA;

[h]Marie-Josée and Henry R. Kravis Center for Molecular Oncology, Memorial Sloan Kettering Cancer Center, New York, NY, USA;

[i]Weizmann Institute of Science, Rehovot, Israel;

[j]Genitourinary Oncology Service, Department of Medicine, Memorial Sloan Kettering Cancer Center, New York, NY, USA;

[k]Department of Radiology, Memorial Sloan Kettering Cancer Center, New York, NY, USA

Abstract

Background and objective: Molecular classification of upper tract urothelial carcinoma (UTUC) can provide insight into divergent clinical outcomes and provide a biological rationale for clinical decision-making. As such, we performed multi-omic analysis of UTUC tumors to identify molecular features associated with disease recurrence and response to immune checkpoint blockade (ICB).

Methods: Targeted DNA and whole transcriptome RNA sequencing was performed on 100 UTUC tumors collected from patients undergoing nephroureterectomy. Consensus non-negative matrix factorization was used to identify molecular clusters associated with clinical outcomes. Gene set enrichment and immune deconvolution analyses were performed. Weighted gene co-expression network analysis was employed for unsupervised identification of gene networks in each cluster.

Key findings and limitations: Five molecular clusters with distinct clinical outcomes were identified. Favorable subtypes (C1 and C2) were characterized by a luminal-like signature and an immunologically depleted tumor microenvironment (TME). Subtype C3 was characterized by *FGFR3* alterations and a higher tumor mutational burden, and included all tumors with microsatellite instability. Despite higher rates of recurrence and inferior survival, subtypes C4 and C5 harbored an immunologically rich TME favoring response to ICB. Limitations include extrapolation of molecular features of tumors from the primary site to determine response to systemic immunotherapy and the limited resolution of bulk sequencing to distinguish gene expression in the tumor, stroma, and immune compartments.

Conclusions and clinical implications: RNA sequencing identified previously underappreciated UTUC molecular heterogeneity and suggests that UTUC patients at the highest risk of metastatic recurrence following surgery include those most likely to benefit from perioperative ICB.

Keywords

Upper tract urothelial cancer; Whole transcriptomic sequencing; Targeted exome sequencing; Molecular clusters; Tumor microenvironment; Immune checkpoint blockade

1. Introduction

Upper tract urothelial carcinoma (UTUC) comprises 5–10% of urothelial tract tumors [1,2]. While there are biological similarities between bladder and upper tract urothelial cancers, these are considered distinct clinical entities with divergent molecular characteristics and management strategies. More specifically, tumor genomic profiling studies have revealed important differences in the somatic mutational landscape of UTUC and bladder urothelial cancers, including a higher prevalence of *FGFR3* and *HRAS* and a lower prevalence of *RB1* and *TP53* alterations in UTUC [3,4]. Although oncogenic mutations in these genes, particularly in *FGFR3* and *TP53*, have been associated with clinical outcomes, differences in somatic mutational profiles are insufficient to explain the variability in cancer-specific survival (CSS) and response to systemic therapy observed in patients with UTUC. Transcriptomic analysis based on RNA sequencing (RNA-seq) may therefore identify complementary molecular biomarkers that better distinguish patients likely to be cured with standard care local and systemic therapies from those at the greatest risk of disease recurence and cancer-related mortality. Such analyses could also uncover new drug targets.

Prior transcriptomic profiling studies of UTUC employed molecular classification schema developed for muscle-invasive bladder cancer (MIBC) and depicted UTUC as a largely homogenous luminal-papillary tumor type [5,6]. We hypothesized that alternative classification schema could identify distinct molecular subtypes of UTUC associated with differences in clinical outcomes. We therefore performed an integrated multi-omic analysis to identify molecular features associated with metastatic disease recurrence in a large cohort of patients with UTUC undergoing nephroureterectomy. Given the expanding role of immune checkpoint blockade (ICB) for the treatment of patients with unresectable and metastatic UTUC, we also sought to evaluate the association between immunological features of the tumor microenvironment (TME) and response to ICB across transcriptionally defined molecular subtypes [7].

2. Patients and methods

A total of 100 UTUC tumors from nephroureterectomy specimens were collected from patients without metastatic disease based on presurgical imaging (MSK100). Representative hematoxylin and eosin slides from frozen tissue and formalin-fixed paraffin-embedded sections were centrally reviewed by a board-certified genitourinary pathologist (H.A.) to confirm histology, grade, and stage. All tissue was collected under protocols approved by the Memorial Sloan Kettering Cancer Center (MSKCC) institutional Review Board (NCT01775072, MSKCC IRB #89–076 and IRB #06–107), and written and verbal informed consents were provided by all participants.

Analysis of patient-matched tumor and normal DNA was performed using the MSK-IMPACT assay, a hybridization capture-based next-generation sequencing assay designed to detect mutations, copy number alterations, and select gene fusions in up to 505 cancer-associated genes [8,9]. Genomic alterations were classified as pathogenic/likely pathogenic based on OncoKB [10], and tumor mutational burden (TMB) was calculated as the number of detected nonsynonymous mutations normalized to the genomic coverage of the respective

MSK-IMPACT panel employed and reported as mutations/megabase (mut/Mb). MSIsensor was used to identify tumors with microsatellite instability (MSI) [11].

RNA was extracted from frozen tumor tissue for RNA-seq. Molecular subtyping based on the MIBC consensus classification schema was performed using The Cancer Genome Atlas (TCGA) MIBC cohort as a comparator [12]. Consensus non-negative matrix factorization (cNMF) analysis was performed using the top 10% most differentially expressed genes to identify molecular clusters [12,13]. The results of differential gene expression analysis were used as input for gene set enrichment analysis (GSEA), and immune deconvolution analysis was employed to define the cell composition of the TME. Differences in gene signatures across molecular clusters were determined using Kruskal-Wallis testing. Weighted gene co-expression network analysis (WGCNA) was performed for unsupervised identification of co-expressed gene networks among samples using the top 10% most differentially expressed genes in the cNMF analysis. RNA-seq was performed on tumors collected from an expansion cohort of UTUC patients treated with ICB ($n = 13$) and combined with 18 patients from the MSK100 cohort treated with ICB following disease recurrence to identify associations between transcriptomic clusters and response to ICB ($n = 31$ total UTUC patients treated with systemic immunotherapy for metastatic disease; Supplementary Table 3).

Clinical annotation was performed manually, and survival outcomes based on molecular features were evaluated using the Kaplan-Meier method with log-rank testing and the Cox-proportional hazards model. Metastatic disease recurrence following nephroureterectomy was defined as recurrence of urothelial cancer involving any metastatic site including retroperitoneal lymph nodes. Urothelial recurrences within the bladder or involving the contralateral upper tract were excluded from this definition. Disease-free survival (DFS) was calculated from the date of initiation of systemic therapy to the date of disease progression or death, whichever occurred first. CSS and overall survival (OS) were calculated from the date of systemic therapy to death based on the cause of death. Progression-free survival (PFS) was calculated from the date of systemic therapy to the date of metastatic recurrence. All survival outcomes were censored at the last encounter in the absence of events. Response to systemic therapy was based on the first axial imaging (CT or MRIcomputed) following initiation of treatment, and differences in response based on gene signatures were evaluated using the Wilcoxon rank sum test. To validate clinical-genomic association identified through analysis of the MSK100 cohort, analyses were repeated using an independent cohort of 158 Japanese patients with UTUC reported by Fujii et al [7].

Further details regarding sequencing, computational, and statistical methods are described in the Supplementary material.

3. Results

To identify molecular features associated with metastatic disease recurrence in patients with localized UTUC treated with nephroureterectomy, we performed whole transcriptome RNA-seq of 100 fresh frozen nephroureterectomy tumor specimens from 100 patients with nonmetastatic UTUC (MSK100), 99 of whom had sufficient tumor tissue for targeted DNA

sequencing using the MSK-IMPACT assay. Patient demographics, clinical features, and transcriptomic molecular classifications based on the consensus classification schema for MIBC are summarized in Figure 1A and Supplementary Table 1 [5]. Consistent with prior studies, luminal (luminal papillary [LumP] and luminal unstable [LumU]) transcriptional profiles were enriched in the MSK100 UTUC cohort, with a LumP transcriptional profile identified in 89% of UTUC tumors versus 32.6% of MIBC cases analyzed by TCGA [12]. Notably, while representing only 8% of tumors in the cohort, basal/squamous, stromarich, and neuroendocrine-like subtypes were enriched in patients who developed metastatic recurrence following surgery (4.17% [two of 48 nonrecurrent group] vs 14.3% [six of 42 recurrent group], $p = 0.066$) by two-sided Fisher's exact test.

Given the limited utility of the MIBC consensus classification schema for predicting metastatic recurrence following nephroureterectomy in patients with UTUC, we performed unsupervised cNMF clustering of RNA-seq data from the MSK100 cohort to identify transcriptional features predictive of cancer-specific outcomes (Fig. 1B). Through an analysis of the top 10% differentially expressed genes ($n = 2260$), UTUC tumors could be divided into five distinct molecular clusters (cluster 1 [C1] = 24, C2 = 11, C3 = 30, C4 = 17, and C5 = 18) with clinically meaningful differences. The likelihood of metastatic recurrence was highest for C5 followed by C4 (Fig. 1C). Consistent with their greater risk of metastatic disease recurrence following surgery, C4 and C5 were associated with higher tumor stage (pT3/pT4 = 58.8% and 72.2%, respectively), whereas C1 was enriched in noninvasive tumors (<pT2 = 83.3%; Supplementary Fig. 1A). Transcriptionally defined subsets were also associated with divergent CSS, with C5 tumors having the shortest CSS followed by C4 ($p = 0.005$; Fig. 1D). Differences in OS were similar, with C1 having the highest OS at 10 yr. To investigate if molecular subtype was prognostic after controlling for previously established clinical and pathological prognostic features, we performed a multiple Cox regression analysis (Supplementary Table 2). Although the univariate analysis demonstrated a strong association between transcriptional subtype C5 and DFS ($p < 0.001$), pT stage was the only relevant factor associated with DFS in multiple Cox regression analysis.

To determine whether the prevalence of oncogenic somatic alterations varied as a function of transcriptional subtype, we integrated RNA-seq data with targeted DNA sequencing data generated using the MSK-IMPACT assay(Fig. 2A). The mean TMB was 16.9 mut/Mb and was highest in C3 (Fig. 2B). Consistent with prior studies, *FGFR3* (48.5%), *TERT* (37.4%), *KDM6A* (23.2%), *KMT2D* (30.3%), and TP53 (23.2%) were the most commonly altered genes [3,4]. To confirm that the somatic mutational landscape of MSK100 cohort was representative of UTUC tumors in general, we compared the mutational profiles of the MSK100 cohort with those of our larger institutional database of patients undergoing nephroureterectomy for UTUC who have had clinical MSK-IMPACT tumor genomic profiling and observed comparable frequencies of common genomic alterations (Supplementary Fig. 2).

Notable genomic differences were observed between molecular clusters. All microsatellite instability high (MSIH, $n = 5$) UTUC tumors were found within the C3 cluster. Of these five tumors, four arose in patients with Lynch syndrome, with the other tumor harboring

a somatic *MSH2* mutation. Oncogenic alterations in *FGFR3* were identified in nearly all C3 tumors (28/30), consistent with previous studies demonstrating an association between high TMB, MSI, and *FGFR3* alterations in urothelial carcinoma (Fig. 2C) [14,15]. Of the 28 tumors, seven were *FGFR3* R248C, an *FGFR3* hotspot mutation previously shown to be enriched in Lynch syndrome–associated UTUC [14]. Patients with *FGFR3* gene alterations had favorable CSS ($p < 0.05$), although statistical significance was not achieved for OS ($p = 0.29$; Fig. 2D). *TP53* mutations were enriched in C2 (54.5%) and C5 (44.4%), and were rare in C1 (8.3%). Alterations in *TP53* were associated with worse CSS ($p < 0.01$) and OS ($p < 0.01$), consistent with prior studies (Fig. 2E) [16].

Although differences in the prevalence of *FGFR3* and *TP53* alterations explain some of the variation in clinical outcomes of patients in the MSK100 cohort, these were insufficient to explain differential outcomes based on transcriptional clustering. As such, we used previously described molecular gene signatures to gain insight into the biology of each cluster [12,17,18]. C1 and C2 had a luminal phenotype, C3 and C4 had a basal/squamous phenotype, and C5 was characterized by mesenchymal features with high expression of myofibroblast, claudin-low, EMT, and p53-like signatures (Fig. 3A). Luminal signatures were associated with superior DFS ($p = 0.004$), whereas transcriptomic features consistent with squamous differentiation ($p = 0.006$), epithelial-mesenchymal transition ($p = 0.001$), claudin-low ($p < 0.001$), and myofibroblast transcriptomic signatures ($p = 0.001$) were associated with inferior DFS. (Supplementary Fig. 3).

To identify molecular processes associated with clinical outcomes, we next performed WGCNA to identify modules of highly correlated genes in an unbiased manner [19]. Based on WGCNA, eight enriched gene modules were identified (Fig. 3B). Notable findings included increased expression of cell cycle/proliferation genes in C2, increased immune infiltration in C4 and C5, and increased angiogenesis-related gene expression in C5. Pathway-based modeling with WGCNA provided further insight into biological differences underlying clinical outcomes in each of the clusters (Supplementary Fig. 4). Cell cycle/proliferation, immune infiltration, and angiogenesis/TGF-β–associated gene expression modules correlated with inferior DFS, whereas genes involved in the processing of organic hydroxyl and hydrogen peroxide compounds were associated with improved DFS (Fig. 3C).

Findings from GSEA and immune deconvolution analysis were next used to explore the immunological phenotypes differentiated by WGCNA (Fig. 3D and Supplementary Fig. 5A). C1 and C2 were characterized by an immunologically cold TME with low expression of inflammatory signatures including IFN-γ and the ImmuneCheckpoint signature, which represents a compilation of immune checkpoint marker genes [20,21]. C3 represented an intermediate immunological phenotype with low natural killer (NK) cell, neutrophil, and mast cell signatures as compared with the more immunologically rich C4 and C5 tumors. C4 was characterized by infiltration of neutrophils and a significantly higher MHC class I antigen presentation machinery (APM1) signature. Enrichment of hallmark inflammation-related signatures including Inflammatory response, Allograft rejection, and IL-6-JAK-STAT3 Signaling were identified by GSEA in both C4 and C5 (Supplementary Fig. 5B). NK cell and Angiogenesis signatures were unique features of the C5 cluster. Both C3 and C5 demonstrated increased infiltration of CD8+ T cells (Supplementary Fig. 5A).

To validate the observed TME characteristics across molecular clusters with an independent cohort, we built a random-forest predictor using the MSK100 cohort as the training dataset with cross-validation and applied it to an independent cohort of 158 transcriptionally profiled UTUC tumors from patients treated in Japan (the Fujii158 cohort) [7]. The pattern of PFS and the T-stage distribution (48% MIBC vs 47.5%) were similar between the MSK100 and Fujii158 cohorts (Fig. 4A and 4B, and Supplementary Fig. 1). TME deconvolution analysis revealed similar patterns of immune features between the MSK100 and Fujii158 cohorts, with higher immune infiltration in the C4 and C5 versus C1 and C2 clusters (Fig. 4C). CD8+ T-cell signals were similarly high in C3 and C5 in both MSK100 and Fujii158. Somatic mutation-based molecular subtypes identified by Fujii et al [7] (hypermutated, TP53/MDM2, RAS, FGFR3, and triple-negative) and their correlation with the expression-based molecular clusters were similarly assessed in the MSK100 cohort (Supplementary Fig. 6). Moderate to weak correlation with phi coefficients of 0.2–0.52 was found between somatic mutation-based molecular subtypes, as defined by Fujii et al [7], and gene expression-based molecular subtypes.

Based on the GSEA and immune deconvolution analysis, we hypothesized that the immunological differences among transcriptional clusters identified by RNA-seq could be predictive of response to systemic immunotherapy administered for recurrent metastatic disease. To evaluate this hypothesis, we analyzed RNA-seq data from 31 UTUC tumors collected from patients with UTUC treated with ICB for metastatic disease, including 18 tumors from the MSK100 cohort and an additional 13 patients with UTUC treated with ICB at MSKCC for which sufficient tumor was available for RNA-seq (C1, $n = 6$; C2, $n = 1$; C3, $n = 7$; C4, $n = 6$; and C5, $n = 11$). The systemic treatment administered, the duration of treatment, and the response to ICB for each patient is summarized in Supplementary Table 3. Figure 5A summarizes the duration of treatment response and disease status for individual patients stratified by the median cytolytic activity (CYT) score, an index of cancer immunity calculated using mRNA expression levels of granzyme (*GZMA*) and perforin (*PRF1*) that has previously been shown to be highly correlated with immune checkpoint marker expression and response to ICB (Supplementary Fig. 7) [22–25]. CYT expression was elevated in C4 and C5, and depleted in C1 and C2 (Supplementary Fig. 5A). In patients with C1 and C2 tumors, no objective responses to ICB were observed, and all but one patient developed progressive disease as best response (Fig. 5B).

Complete responses were observed only in patients with the C3 and C5 transcriptional subtypes. Notably, CD8+ T cells were enriched in C3 (Fig. 3D), which had the highest TMB of the five molecular subtypes and demonstrated the best objective response rate to ICB. In addition to the presence of CD8+ T cells, expression of antigen processing machinery (APM) genes, which has been shown to be predictive of response to ICB in numerous cancer types, was significantly associated with objective response in UTUC ($p = 0.04$; Fig. 5C) [26]. The antigen processing and presentation machinery 1 (APM1) signature was enriched in the C4, in which two of seven patients experienced a partial response to ICB, whereas the APM2 signature was enriched in both C4 and C5 (Supplementary Fig. 5A). PD-L1 expression was higher among ICB responders, although this association was not statistically significant. Figure 5D highlights two cases (one MSI-H and one microsatellite stable) of exceptional response to ICB.

4. Discussion

UTUC is an aggressive malignancy in need of advances in prognostic and predictive biomarker identification, drug development, and multimodality clinical management strategies. Molecular characterization of UTUC has lagged bladder urothelial cancer, for which there have been multiple large integrated sequencing studies that are now informing clinical trial design and patient management [5,12,27–31]. To address this gap, we performed whole transcriptome RNA sequencing and targeted DNA sequencing of UTUC tumors from patients undergoing curative-intent nephroureterectomy to identify molecular features associated with metastatic recurrence and other cancer-associated clinical outcomes.

Our analysis identified five transcriptional subtypes with divergent molecular phenotypes, survival outcomes, and response to systemic ICB. C1-C3 were associated with lower-stage disease (<pT2) and favorable survival, whereas C4 and C5 were associated with locally advanced disease (>pT2) and poor survival. Biologically relevant gene expression signatures, including gene expression signatures shown previously to be predictive of ICB response in other cancer types, varied widely across the different clusters, challenging previous views of UTUC as a largely homogenous luminal-like disease [5,6,32]. For example, tumors in the C4 and C5 had molecular features similar to the “luminal infiltrated” TCGA subtype, which has previously been reported to be associated with response to the anti–PD-L1 antibody atezolizumab [12,33].

The current study highlights the complementary nature of DNA- and RNA-based molecular profiling. As a notable example, *TP53* alterations, which were associated with inferior outcomes across the cohort as a whole, were highest in C2, despite this subtype being associated with relatively favorable CSS [34]. Similarly, while *FGFR3* mutant tumors in the MSK100 were more likely to have an expression signature consistent with a cold tumor immune microenvironment, consistent with prior work by Robinson et al [6], *FGFR3* mutation was not predictive of ICB response in the larger cohort of urothelial cancer patients at MSKCC treated with systemic immunotherapy (Supplementary Fig. 8). These and previously published results suggest that *FGFR3* mutant tumors represent a highly heterogeneous subset of urothelial cancers and that co-occurring molecular features such as microsatellite instability and not *FGFR3* mutational status are the likely basis for immune checkpoint inhibitor sensitivity in those patients with *FGFR3* mutant tumors who respond to systemic ICB [14,15,35,36].

It is well established that the TME plays a critical role in tumor pathogenesis and treatment response, but the TME features associated with disease recurrence and systemic therapy response in UTUC have not been well described until recently [7,32,37,38]. Perhaps the most notable finding of the current study was the stark contrast between the “immune-desert” phenotype in low-risk clusters C1 and C2 and the “immune-inflamed” phenotype in high-risk clusters C4 and C5—findings that were consistent across GSEA, WGCNA, and immune deconvolution analysis. Similar immune phenotypes were observed in a recent transcriptomic analysis in which nearly half (46%) of UTUC tumors demonstrated an active immunological phenotype [7]. These phenotypes have been shown to be associated with response to ICB in bladder cancer, although this has not been directly evaluated in UTUC

prior to our study [27]. Of clinical relevance, the proinflammatory state of C4 and C5 may be serendipitous, as the UTUC clusters with transcriptional features associated with inferior clinical outcomes were also those with biological features predictive of response to systemic ICB. For example, as demonstrated in other cancer types, the relatively simple CYT score, which is based on the expression of perforin and granzyme activity, was highest in C4 (median 4.47, interquartile range [IQR] 1.97–6.86) and C5 (median 5.24, IQR 2.01–11.49), which we found to be enriched for objective responses to ICB, warranting further evaluation of CYT score as a predictive biomarker of ICB response in patients with UTUC [22–26].

The strengths of our study included validation of molecular and clinical associations using a second cohort of patients with UTUC, which were analyzed by DNA and RNA sequencing for which clinical outcomes data were available [7]. Our study was, however, limited by the clinical heterogeneity of the MSK100 cohort, including the inclusion of both low- and high-grade tumors and tumors that had previously been exposed to neoadjuvant chemotherapy. An additional limitation was the relatively small number of patients treated subsequently with ICB following disease recurrence and the extrapolation of primary site TME features as defined by RNA-seq to response of metastatic disease sites to ICB [38]. The use of bulk transcriptomic sequencing also has limited resolution for distinguishing gene expression differences arising from the tumor, stroma, and immune compartments, which could potentially be studied in greater depth using newer single-cell sequencing and spatial profiling methods.

Tumors also evolve over time, and the optimal timing of molecular testing will need to be evaluated as part of future studies. While the limitations of current RNA-seq methods suggest that RNA-based molecular profiling will likely need to be performed using high-quality tumors collected from tumor biopsies of the primary site or surgical resections, serial analyses of RNA expression profiles may in the future be feasible using minimally invasive approaches such as circulating tumor cell analyses and exosome profiling. Future transcriptomic analyses of UTUC tumors should also seek to identify biomarkers of response to antibody-drug conjugates targeting Nectin-4, Trop2, and HER2, given the recently reported activity of these agents alone and in combination with ICB in patients with metastatic urothelial cancers [39,40].

5. Conclusions

Integrated RNA and DNA sequencing analysis revealed that UTUC is a molecularly heterogeneous cancer with biological differences driving divergent clinical outcomes. Transcriptional profiling identified molecular subtypes associated to with distinct clinical and biological features, supporting a potential role for RNA-seq as a guide to clinical management in patients with UTUC. As the UTUC transcriptional subtypes with the highest risk of metastatic disease recurrence following curative-intent surgical resection were those with an inflamed TME, our data provide rationale for the evaluation of transcriptomic profiling to identify those UTUC patients at increased risk for metastatic recurrence and those most likely to benefit from ICB for trials of adjuvant or neoadjuvant immunotherapy.

Supplementary Material

Refer to Web version on PubMed Central for supplementary material.

Acknowledgments:

We thank the members of the MSKCC Integrated Genomics Organization Core, which is funded by the NCI Cancer Center Support Grant (CCSG, P30 CA08748).

Funding/Support and role of the sponsor:

This work was supported by MSKCC and Weill Cornell Medicine. Funding was provided by the Thompson Family Foundation, Department of Defense Translational Team Science Award (W81XWH-20-1-0722), SPORE in Bladder Cancer P50-CA221745, Cycle for Survival, NIH T32 National Research Service Award, and the Marie-Josée and Henry R. Kravis Center for Molecular Oncology.

Financial disclosures:

Jonathan A. Coleman certifies that all conflicts of interest, including specific financial interests and relationships and affiliations relevant to the subject matter or materials discussed in the manuscript (eg, employment/affiliation, grants or funding, consultancies, honoraria, stock ownership or options, expert testimony, royalties, or patents filed, received, or pending), are the following: Andrew B. Katims received ASCO Young investigator award. David H. Aggen is a consultant and/or an advisor for Adaptimmune, Astellas, BMS, Century Therapeutics, and Pfizer, and has received research funding from Astellas, Merck, and Pfizer. Eugene J. Pietzak is a consultant and/or an advisor for Merck, Chugai Pharma, QED Therapeutics, Janssen, Urogen Pharma, and CG Oncology, and received research funding from Janssen. Benjamin Greenbaum has received honoraria for speaking engagements from Merck, Bristol Meyers Squibb, and Chugai Pharmaceuticals; has received research funding from Bristol Meyers Squibb and Merck; and has been a compensated consltant for Darwin Health, Merck, PMV Pharma, Shennon Biotechnologies Synteny.ai, and Rome Therapeutics, of which he is a cofounder. Gopa Iyer is a consultant and/or an advisor for Janssen, Mirati Therapeutics, Flare Therapeutics, Loxo/Lilly, and Bicycle Therapeutics; received research funding from Novartis, Debiopharm Group, Bayer, Janssen, and Seagen; and is a member of the speakers' bureau for Gilead Sciences and the Lynx Group. Hikmat Al-Ahmadie is a consultant and/or an advisor for AstraZeneca, PAIGE.AI, and Pfizer. Taha Merghoub is a consultant for Immunos Therapeutics, Daiichi Sankyo Co, TigaTx, Normunity, and Pfizer; is a cofounder of and an equity holder in IMVAQ Therapeutics; receives research funding from Bristol-Myers Squibb and Realta; and is an inventor on patent applications related to work on oncolytic viral therapy, alpha virus–based vaccine, neoantigen modeling, CD40, GITR, OX40, PD-1, and CTLA-4. David B. Solit has consulted for or received honoraria from Rain, Pfizer, Fog Pharma, PaigeAI, BridgeBio, Scorpion Therapeutics, FORE Therapeutics, Function Oncology, Pyramid, Elsie Biotechnologies, Inc, and Meliora Therapeutics, Inc.

References

[1]. Roupret M, Babjuk M, Comperat E, et al. European Association of Urology guidelines on upper urinary tract urothelial cell carcinoma: 2015 update. Eur Urol 2015;68:868–79. [PubMed: 26188393]

[2]. Siegel RL, Miller KD, Jemal A. Cancer statistics, 2016. CA Cancer J Clin 2016;66:7–30. [PubMed: 26742998]

[3]. Audenet F, Isharwal S, Cha EK, et al. Clonal relatedness and mutational differences between upper tract and bladder urothelial carcinoma. Clin Cancer Res 2019;25:967–76. [PubMed: 30352907]

[4]. Sfakianos JP, Cha EK, Iyer G, et al. Genomic characterization of upper tract urothelial carcinoma. Eur Urol 2015;68:970–7. [PubMed: 26278805]

[5]. Kamoun A, de Reynies A, Allory Y, et al. A consensus molecular classification of muscle-invasive bladder cancer. Eur Urol 2020;77:420–33. [PubMed: 31563503]

[6]. Robinson BD, Vlachostergios PJ, Bhinder B, et al. Upper tract urothelial carcinoma has a luminal-papillary T-cell depleted contexture and activated FGFR3 signaling. Nat Commun 2019;10:2977. [PubMed: 31278255]

[7]. Fujii Y, Sato Y, Suzuki H, et al. Molecular classification and diagnostics of upper urinary tract urothelial carcinoma. Cancer Cell 2021;39:793–809, e8. [PubMed: 34129823]

[8]. Bajorin DF, Witjes JA, Gschwend JE, et al. Adjuvant nivolumab versus placebo in muscle-invasive urothelial carcinoma. N Engl J Med 2021;384:2102–14. [PubMed: 34077643]

[9]. Teo MY, Guercio BJ, Pietzak EJ, et al. Neoadjuvant nivolumab (N) + ipilimumab (I) in cisplatin-ineligible patients with upper tract urothelial cancer (UTUC). J Clin Oncol 2023;41:511.

[10]. Chakravarty D, Gao J, Phillips SM, et al. OncoKB: a precision oncology knowledge base. JCO Precis Oncol 2017;2017, PO.17.00011.

[11]. Middha S, Zhang L, Nafa K, et al. Reliable pan-cancer microsatellite instability assessment by using targeted next-generation sequencing data. JCO Precis Oncol 2017;2017, PO.17.00084.

[12]. Robertson AG, Kim J, Al-Ahmadie H, et al. Comprehensive molecular characterization of muscle-invasive bladder cancer. Cell 2017;171:540–556.e25. [PubMed: 28988769]

[13]. Gaujoux R, Seoighe C. A flexible R package for nonnegative matrix factorization. BMC Bioinformatics 2010;11:367. [PubMed: 20598126]

[14]. Donahue TF, Bagrodia A, Audenet F, et al. Genomic characterization of upper-tract urothelial carcinoma in patients with Lynch syndrome. JCO Precis Oncol 2018;2018, PO.17.00143.

[15]. Alam SM, Teo MY, Woo J, et al. Defining molecular features associated with microsatellite instability and response to immune checkpoint blockade in urothelial carcinoma. J Clin Oncol 2024;42:536.

[16]. Mitchell S, Mayer E, Patel A. Expression of p53 in upper urinary tract urothelial carcinoma. Nat Rev Urol 2011;8:516–22. [PubMed: 21811225]

[17]. Fu J, Li K, Zhang W, et al. Large-scale public data reuse to model immunotherapy response and resistance. Genome Med 2020;12:21. [PubMed: 32102694]

[18]. Motzer RJ, Banchereau R, Hamidi H, et al. Molecular subsets in renal cancer determine outcome to checkpoint and angiogenesis blockade. Cancer Cell 2020;38:803–17, e4. [PubMed: 33157048]

[19]. Langfelder P, Horvath S. WGCNA: an R package for weighted correlation network analysis. BMC Bioinformatics 2008;9: 559. [PubMed: 19114008]

[20]. Rodig SJ, Gusenleitner D, Jackson DG, et al. MHC proteins confer differential sensitivity to CTLA-4 and PD-1 blockade in untreated metastatic melanoma. Sci Transl Med 2018;10:eaar3342. [PubMed: 30021886]

[21]. Nixon BG, Kuo F, Ji L, et al. Tumor-associated macrophages expressing the transcription factor IRF8 promote T cell exhaustion in cancer. Immunity 2022;55:2044–58, e5 [PubMed: 36288724]

[22]. Mezheyeuski A, Backman M, Mattsson J, et al. An immune score reflecting pro- and anti-tumoural balance of tumour microenvironment has major prognostic impact and predicts immunotherapy response in solid cancers. EBioMedicine 2023;88:104452. [PubMed: 36724681]

[23]. Chen Q, Wang C, Lei X, Huang T, Zhou R, Lu Y. Immune cytolytic activity for comprehensive insights of the immune landscape in endometrial carcinoma. J Oncol 2022;2022:9060243. [PubMed: 35898926]

[24]. Hu Q, Nonaka K, Wakiyama H, et al. Cytolytic activity score as a biomarker for antitumor immunity and clinical outcome in patients with gastric cancer. Cancer Med 2021;10:3129–38. [PubMed: 33769705]

[25]. Rooney MS, Shukla SA, Wu CJ, Getz G, Hacohen N. Molecular and genetic properties of tumors associated with local immune cytolytic activity. Cell 2015;160:48–61. [PubMed: 25594174]

[26]. Thompson JC, Davis C, Deshpande C, et al. Gene signature of antigen processing and presentation machinery predicts response to checkpoint blockade in non-small cell lung cancer (NSCLC) and melanoma. J Immunother Cancer 2020;8:e000974. [PubMed: 33028693]

[27]. Robertson AG, Meghani K, Cooley LF, et al. Expression-based subtypes define pathologic response to neoadjuvant immune-checkpoint inhibitors in muscle-invasive bladder cancer. Nat Commun 2023;14:2126. [PubMed: 37105962]

[28]. Strandgaard T, Lindskrog SV, Nordentoft I, et al. Elevated T-cell exhaustion and urinary tumor DNA levels are associated with bacillus Calmette-Guerin failure in patients with non-muscle-invasive bladder cancer. Eur Urol 2022;82:646–56. [PubMed: 36210217]

[29]. Taber A, Christensen E, Lamy P, et al. Molecular correlates of cisplatin-based chemotherapy response in muscle invasive bladder cancer by integrated multi-omics analysis. Nat Commun 2020;11:4858. [PubMed: 32978382]

[30]. Lindskrog SV, Prip F, Lamy P, et al. An integrated multi-omics analysis identifies prognostic molecular subtypes of non-muscle-invasive bladder cancer. Nat Commun 2021;12:2301. [PubMed: 33863885]

[31]. Griffin J, Down J, Quayle LA, et al. Verification of molecular subtyping of bladder cancer in the GUSTO clinical trial. J Pathol Clin Res 2024;10:e12363.

[32]. Califano G, Ouzaid I, Laine-Caroff P, et al. Current advances in immune checkpoint inhibition and clinical genomics in upper tract urothelial carcinoma: state of the art. Curr Oncol 2022;29:687–97. [PubMed: 35200559]

[33]. Rosenberg JE, Hoffman-Censits J, Powles T, et al. Atezolizumab in patients with locally advanced and metastatic urothelial carcinoma who have progressed following treatment with platinum-based chemotherapy: a single-arm, multicentre, phase 2 trial. Lancet 2016;387:1909–20. [PubMed: 26952546]

[34]. Lee JY, Cho KS, Diaz RR, Choi YD, Choi HY. p53 expression as a prognostic factor in upper urinary tract urothelial carcinoma: a systematic review and meta-analysis. Urol Int 2015;94:50–7. [PubMed: 25171290]

[35]. Loriot Y, Necchi A, Park SH, et al. Erdafitinib in locally advanced or metastatic urothelial carcinoma. N Engl J Med 2019;381:338–48. [PubMed: 31340094]

[36]. Rose TL, Weir WH, Mayhew GM, et al. Fibroblast growth factor receptor 3 alterations and response to immune checkpoint inhibition in metastatic urothelial cancer: a real world experience. Br J Cancer 2021;125:1251–60. [PubMed: 34294892]

[37]. Jardim DL, Goodman A, de Melo GD, Kurzrock R. The challenges tumor mutational burden as an immunotherapy biomarker. Cancer Cell 2021;39:154–73. [PubMed: 33125859]

[38]. Ohara K, Rendeiro AF, Bhinder B, et al. The evolution of metastatic upper tract urothelial carcinoma through genomic-transcriptomic and single-cell protein markers analysis. Nat Commun 2024;15:2009. [PubMed: 38499531]

[39]. Hoimes CJ, Flaig TW, Milowsky MI, et al. Enfortumab vedotin plus pembrolizumab in previously untreated advanced urothelial cancer. J Clin Oncol 2022;41:22–31. [PubMed: 36041086]

[40]. Powles T, Rosenberg JE, Sonpavde GP, et al. Enfortumab vedotin in previously treated advanced urothelial carcinoma. N Engl J Med 2021;384:1125–35. [PubMed: 33577729]

[41]. Stagg J, Smyth MJ. Extracellular adenosine triphosphate and adenosine in cancer. Oncogene 2010;29:5346–58. [PubMed: 20661219]

ADVANCING PRACTICE

What does this study add?

Integrated DNA and RNA sequencing of upper tract urothelial carcinoma (UTUC) tumors revealed that tumors with transcriptional features associated with unfavorable survival are more likely to have an immune-rich tumor microenvironment predictive of an immune checkpoint inhibitor response. The study highlights previously underappreciated molecular heterogeneity in UTUC identifiable by RNA but not DNA sequencing and suggests that UTUC patients at the highest risk of recurrence may be those most likely to benefit from perioperative immunotherapy. The data support adjuvant clinical trials of immune checkpoint blockade in clinically and molecularly defined subsets of UTUC patients, with the goal of reducing the risk of metastatic disease recurrence.

Clinical Relevance

This study identifies distinct molecular signatures in upper tract urothelial carcinoma with immune-enriched tumor microenvironments that may be more likely to respond to immune checkpoint blockade therapy. These findings support a personalized approach to perioperative therapy, rather than a one-size-fits-all model, potentially reducing recurrence risk and improving survival in high-risk UTUC patients. Associate Editor: Laura Bukavina.

Patient Summary

This study highlights the molecular heterogeneity of upper tract urothelial cancer (UTUC) and suggests that tumor molecular profiling could identify patients at the greatest risk of progression to metastatic disease, the lethal disease state. The study also suggests that UTUC patients at the highest risk of recurrence may be those most likely to benefit from perioperative immunotherapy and support future clinical trials in which molecular analyses are used to identify the risk of recurrence and guide treatment intensification, including adjuvant immunotherapy, for patients at the greatest risk of cancer-specific mortality.

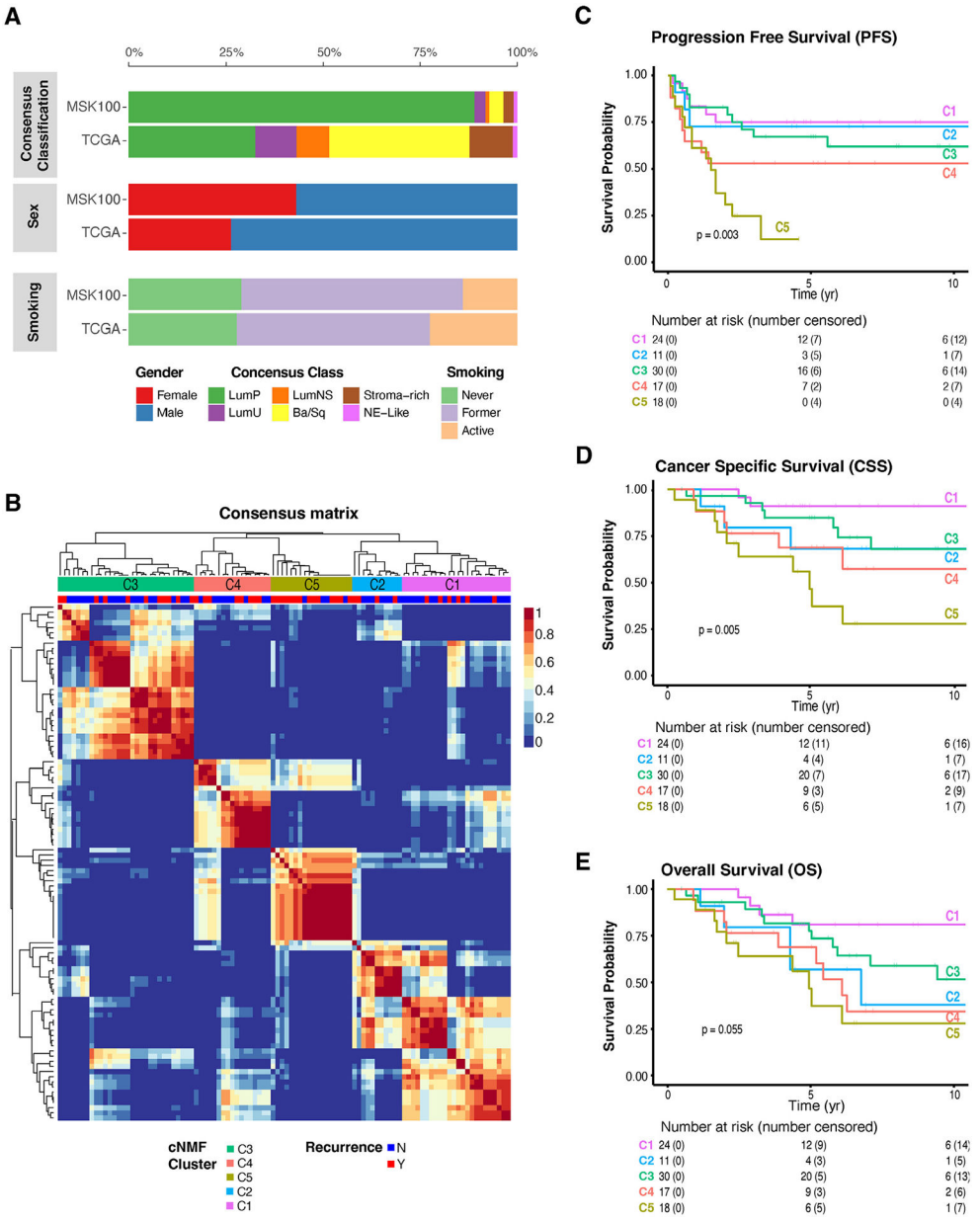

Fig. 1 –.

Whole transcriptomic analysis of UTUC tumors identifies five molecular clusters associated with clinical outcomes. (A) Clinical characteristics and transcriptional profiles based on the consensus classification schema for bladder cancers developed by the Bladder Cancer Molecular Taxonomy Group for 100 UTUC tumors (MSK100 cohort) and The Cancer Genome Atlas (TCGA) muscle-invasive bladder urothelial carcinoma cohort. (B) Clustering analysis of RNA-seq data for the MSK100 cohort based on consensus non-negative matrix factorization (cNMF) revealed five distinct clusters (C1: $n = 24$; C2: $n = 11$; C3: $n = 30$; C4: $n = 17$; and C5: $n = 18$). The top 10% of most varied genes ($n = 2260$ genes) determined by median absolute deviation were used for cNMF analysis. (C) Progression-free survival showing the association of transcriptional subtypes and metastatic recurrence. Recurrence

was defined as any metastatic disease recurrence following nephroureterectomy. (D) Cancer-specific survival and (E) overall survival based on transcriptional subtype. The median time frame of the follow-up period post-nephroureterectomy was 60 mo, and IQR was 32.3–86.3 mo. Ba/Sq = basal/squamous; IQR = interquartile range; LumNS = luminal nonspecified; LumP = luminal papillary; LumU = luminal unstable; N = no; NE = neuroendocrine; RNA-seq = RNA sequencing; UTUC = upper tract urothelial carcinoma; Y = yes.

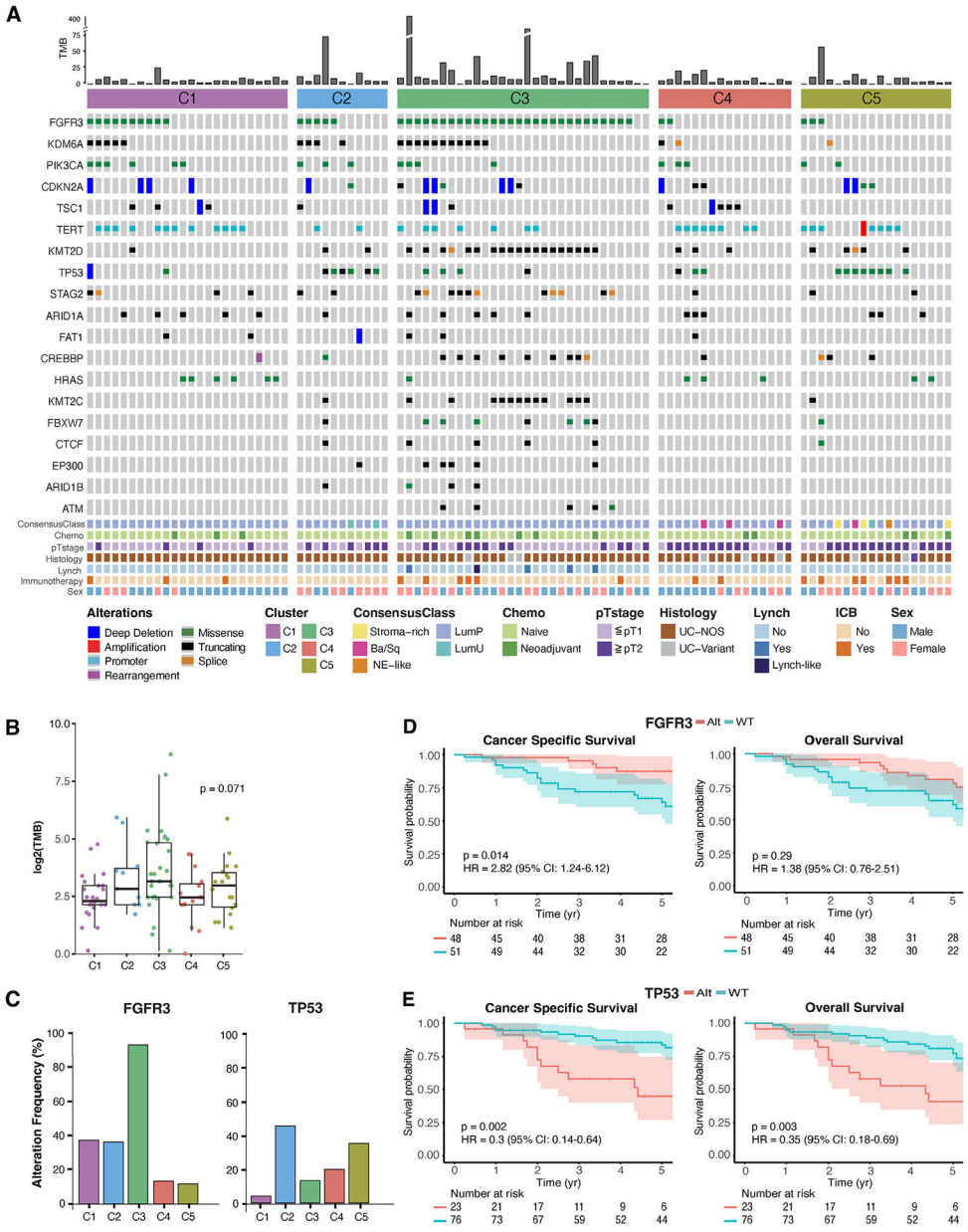

Fig. 2 –.

Integrated analysis of DNA and RNA sequencing of UTUC tumors identifies differences in somatic mutational profiles among transcriptionally defined molecular clusters. (A) Oncoprint showing oncogenic/likely oncogenic somatic alterations in select frequently mutated genes in the MSK100 cohort. Samples were grouped based on the five transcriptomic clusters identified in Figure 1. (B) Mean tumor mutation burden of each transcriptionally defined cluster. The box represents the interquartile range (IQR) and the line indicates the median. Whiskers extend from the box to the smallest and largest values within 1.5 times the IQR from the lower and upper quartiles, respectively, delineating the range of typical data values. (C) Frequency of *FGFR3* and *TP53* mutations as a function of transcriptomic cluster. *FGFR3* mutations were most common in C3 (93%), whereas *TP53*

mutations were most common in C2 (55%) and C5 (47%). Clinical outcome as a function of (D) *FGFR3* and (E) *TP53* mutational status. DNA sequencing results were not available for one tumor in the C2 cluster due a lack of sufficient tissue. Ba/Sq = basal/squamous; CI = confidence interval; HR = hazard ratio; ICB = immune checkpoint blockade; LumP = luminal papillary; LumU = luminal unstable; NE = neuroendocrine; NOS = not otherwise specified; TMB = tumor mutational burden.

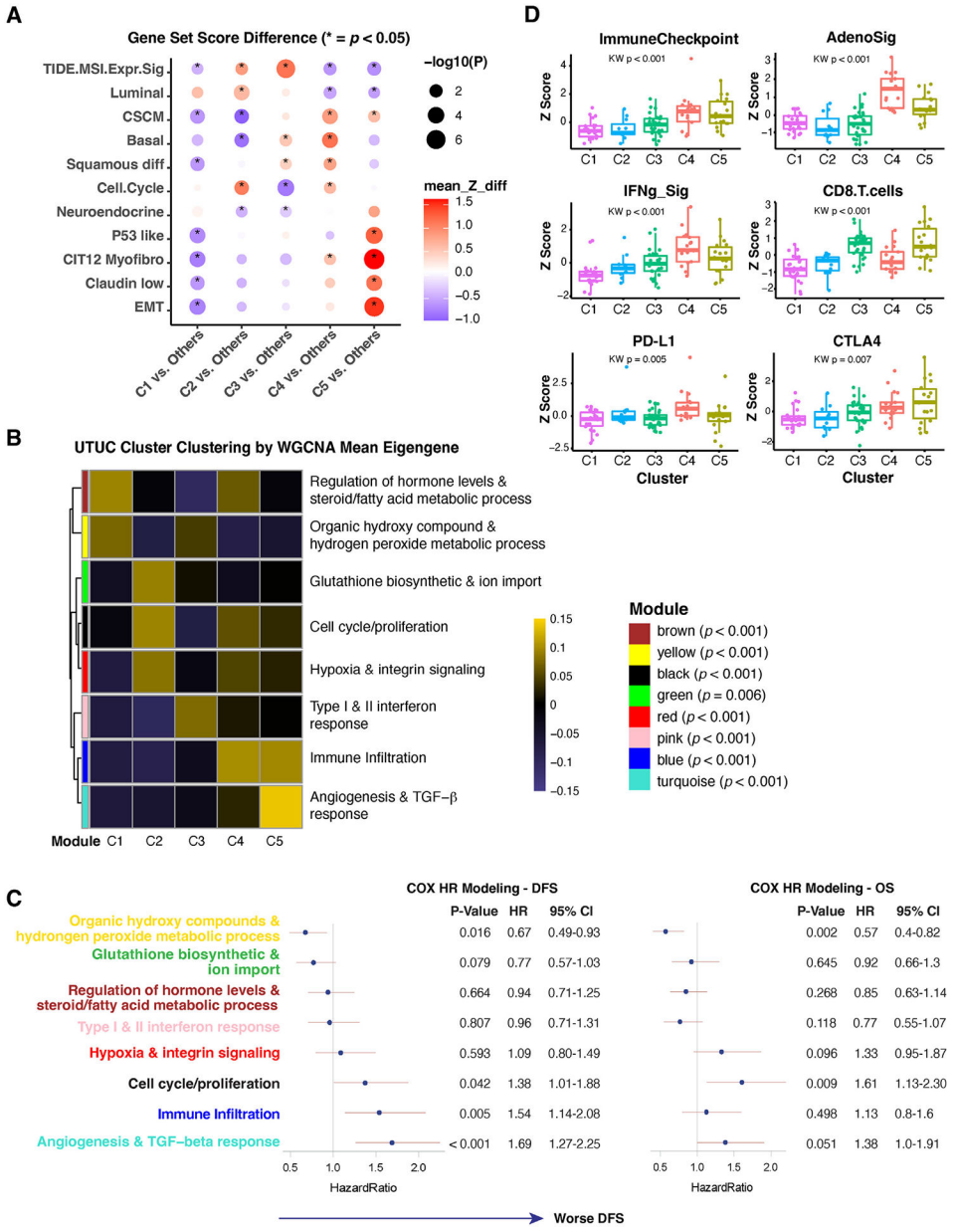

Fig. 3 –.

Increased immune infiltration in transcriptional clusters associated with a higher risk for disease recurrence following nephroureterectomy. (A) Tumor intrinsic characteristics of each transcriptional cluster. (B) Weighted correlation network analysis (WGCNA) heatmap demonstrating gene set expression as a function of transcriptional subtypes. (C) Association between gene modules and disease-free and overall survival. (D) Immune signatures derived from immune deconvolution analysis stratified by clusters: p value by Kruskal-Wallis (KW) test. The ImmuneCheckpoint signature, which includes immune checkpoint blockade target genes including CTLA-4, LAG-3, PD-1, PD-L1, PD-L2, TIM3, and TIGIT, was used for evaluating potential immune checkpoint signaling based on RNA-seq analysis [21]. The immune marker signature scores including ImmuneCheckpoint, IFN-γ, CD8 T cells, PD-L1,

CTLA4, and AdenoSig were derived through single-sample gene set enrichment analysis. AdenoSig is a signature of adenosine signaling, which has been associated with suppression of NK and CD8 function and recruitment of immunosuppressive cells [41]. CI = confidence interval; DFS = disease-free survival; HR = hazard ratio; NK = natural killer cell..

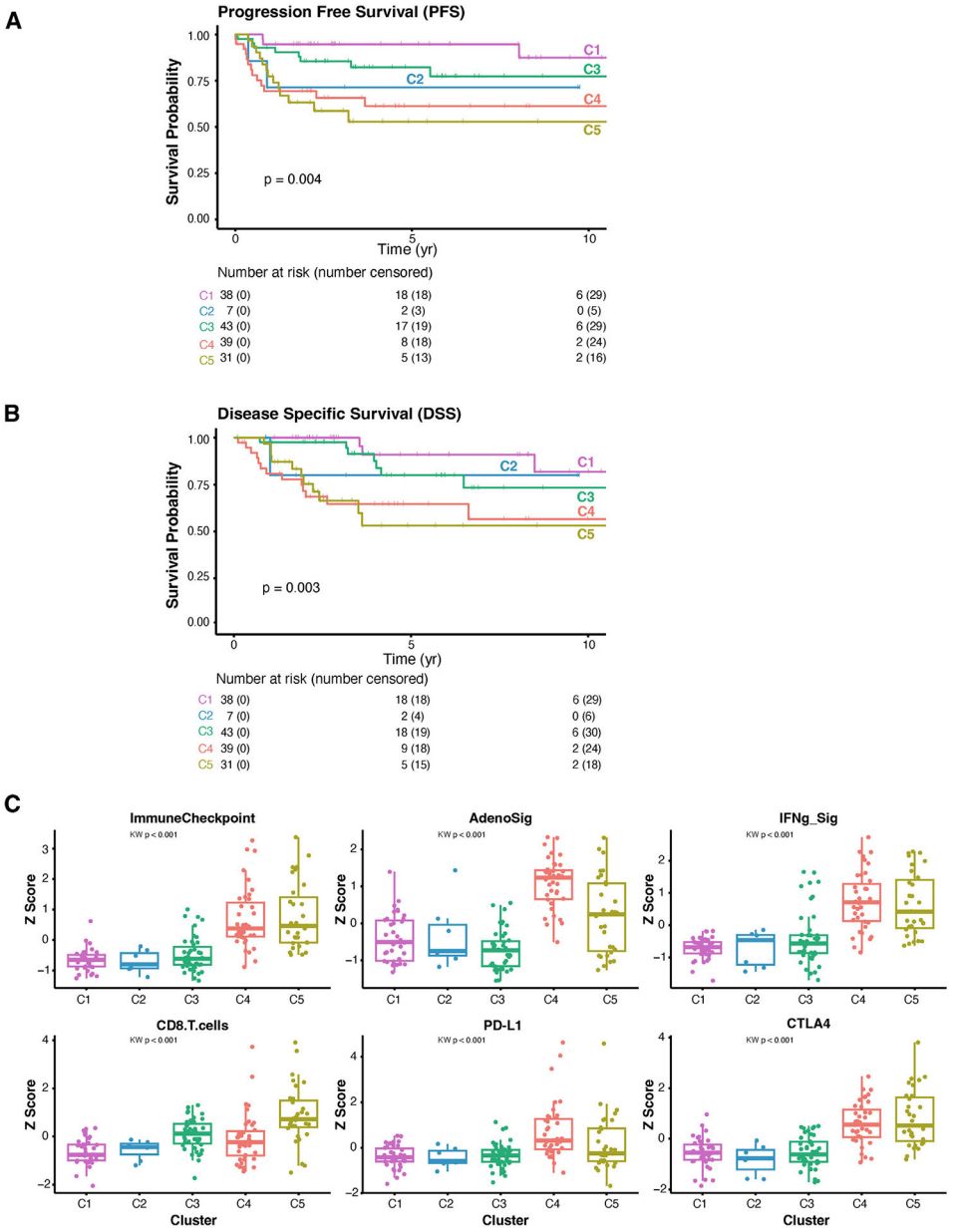

Fig. 4 –.

Comparison of the MSK100 and Fujii158 cohorts. (A) Progression-free survival showing the association of transcriptional subtypes and metastatic recurrence. (B) A Kaplan-Meier plot of DSS as a function of transcriptional clusters for the 158 UTUC tumors in the Fujii et al [7] cohort. DSS, not CSS, was utilized, as only DSS was reported for the Fujii et al's [7] cohort. (C) Select immune features as a function of transcriptional cluster for tumors in the Fujii et al's [7] cohort. A log transformed expression matrix of the top 10% most varied genes that were included in the cNMF molecular clustering was built by integrating the RNA sequencing data from the MSK100 cohort, the 13 patients in the immune checkpoint inhibitor–treated expansion cohort, and the 158 patients in the Fujii158 cohort after batch correction using the ComBat function from the Rsva package. cNMF =

consensus non-negative matrix factorization; CSS = cancer-specific survival; DSS = disease-specific survival.

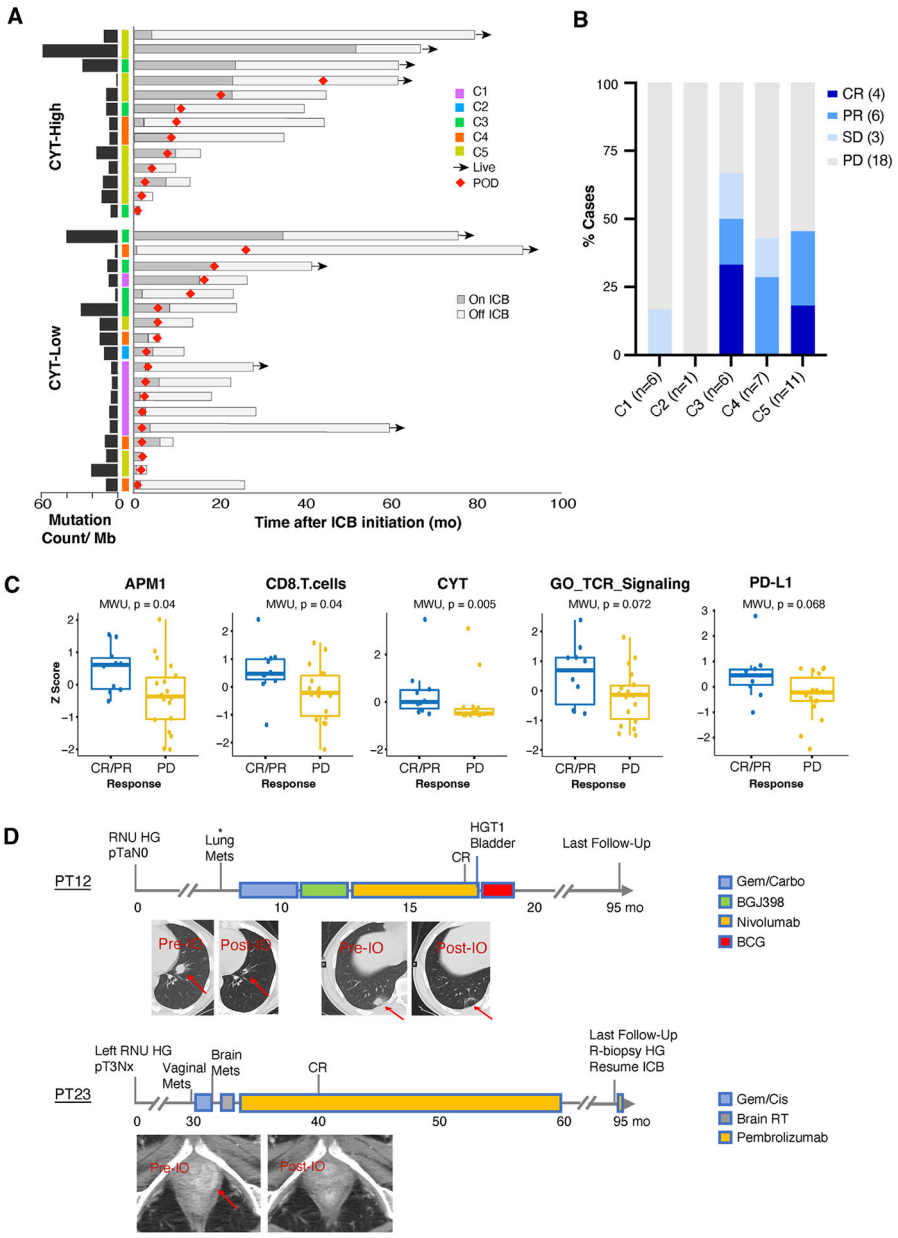

Fig. 5 –.

Molecular phenotypes are associated with divergent response to immune checkpoint blockade (ICB) in metastatic UTUC. (A) A swimmer's plot depicting the clinical response of individual patients with UTUC to ICB treatment for metastatic disease. Patient responses were ordered using the cytolytic activity (CYT) score inferred from RNA sequencing data, and progression of disease (POD) was determined by imaging. The CYT score was calculated based on the mRNA expression levels of granzyme A (GZMA) and perforin (PRF1). The median of the CYT score was 2.265 and used for the CYT-high cutoff. Tumor mutation count is shown on the left. Arrows represent patients who are alive at the time of last assessment. (B) Clinical response of patients with UTUC to ICB stratified by transcriptional cluster. The median time frame of the first axial imaging following

initiation of treatment when determining CR/PR/SD/PD was 9.7 wk (IQR 7.4–11.6 wk). (C) Enrichment of immune effector cell infiltration among patients with CR/PR (n = 10) compared with those with PD (n = 18). For two-group comparison, Mann-Whitney U test (Wilcoxon-Mann-Whitney U test) was used. (D) Disease course and systemic therapies received for two patients with UTUC who had durable responses to ICB. PT12 ([cluster 5], TMB-H [10.8], microsatellite stable) was treated with gemcitabine/carboplatin (Gem/Carbo), BGJ398, and nivolumab followed by intravesical BCG for a subsequent high-grade T1 bladder lesion. BGJ398 was discontinued because of toxicity (abnormal kidney function). PT23 ([cluster 3], TMB-H [27.5], MSI-H), in the setting of Lynch syndrome, was treated with gemcitabine/cisplatin (Gem/Cis) and radiation therapy for brain metastasis, followed by pembrolizumab. Treatment with pembrolizumab was recently resumed after the patient developed a urothelial tumor in the right ureter. BCG = bacillus Calmette-Guerin; CR = complete response; IQR = interquartile range; MSI-H = microsatellite instability high; PD = progression of disease; PR = partial response; RT = radiation therapy; SD = stable disease; TMB = tumor mutational burden.